Acta Pharmaceutica Sinica B 2021;11(6):1592−1606

Chinese Pharmaceutical Association
Institute of Materia Medica, Chinese Academy of Medical Sciences

Acta Pharmaceutica Sinica B

www.elsevier.com/locate/apsb
www.sciencedirect.com

ORIGINAL ARTICLE

HYD-PEP06 suppresses hepatocellular carcinoma metastasis, epithelial−mesenchymal transition and cancer stem cell-like properties by inhibiting PI3K/AKT and WNT/β-catenin signaling activation

Wei Tian[a,†], Jiatong Li[a,†], Zhuo Wang[a,†], Tong Zhang[b], Ying Han[a], Yanyan Liu[c], Wenfeng Chu[a], Yu Liu[a,*], Baofeng Yang[a,*]

[a]*Department of Pharmacology (the State-Province Key Laboratories of Biomedicine Pharmaceutics of China, Key Laboratory of Cardiovascular Research, Ministry of Education), College of Pharmacy, Harbin Medical University, Harbin 150081, China*
[b]*The First Affiliated Hospital of Harbin Medical University, Harbin 150081, China*
[c]*Translational Medicine Research and Cooperation Center of Northern China, Heilongjiang Academy of Medical Sciences, Harbin 150081, China*

Received 3 November 2020; received in revised form 27 February 2021; accepted 12 March 2021

KEY WORDS

Hepatocellular carcinoma;
HYD-PEP06;
Cancer stem-like cell;
PI3K/AKT;
WNT/β-catenin

Abstract HYD-PEP06, an endostatin-modified polypeptide, has been shown to produce effective anti-colorectal carcinoma effects through inhibiting epithelial−mesenchymal transition (EMT). However, whether HYD-PEP06 has similar suppressive effect on hepatocellular carcinoma (HCC) remained unknown. In this study, HYD-PEP06 inhibited metastasis and EMT but not proliferation *in vitro*. Cignal finder pathway reporter array and Western blot analysis revealed that HYD-PEP06 suppressed HCCLM3 cell metastasis and EMT by inhibiting the PI3K/AKT pathway. Moreover, HYD-PEP06 exerted anti-metastasis effects in HepG2 cancer stem-like cells (CSCs) *via* suppressing the WNT/β-catenin signaling pathway. Finally, in HCCLM3 tumor-bearing BALB/c *nu/nu* nude mice, HYD-PEP06 substantially

*Corresponding authors. Tel.: +86 451 86671354; fax: +86 451 86675769.
E-mail addresses: hmu_ly@163.com (Yu Liu), yangbf@ems.hrbmu.edu.cn (Baofeng Yang).
†These authors made equal contributions to this work.
Peer review under responsibility of Chinese Pharmaceutical Association and Institute of Materia Medica, Chinese Academy of Medical Sciences.

https://doi.org/10.1016/j.apsb.2021.03.040

suppressed tumor growth, lung metastasis and HCC progress. Our results suggest that HYD-PEP06 inhibits the metastasis and EMT of HCC and CSCs as well, and thus has the potential as an agent for HCC treatment.

1. Introduction

Hepatocellular carcinoma (HCC), as one of the most worldwide malignancies, makes up of 90% primary liver cancer and its incidence continues to rise worldwide[1]. Surgical removal of nidus is the major strategy for HCC, accompanied by high recurrence rate and intrahepatic and extrahepatic metastasis. Sorafenib, a novel multi-targeted oral drug, was authorized as a unique target medicament for advanced HCC by the U.S. Food and Drug Administration in 2007, and it acts by attenuating tumor angiogenesis, delaying tumor progress and inducing apoptosis[2,3]. However, due to the development of resistance of HCC to sorafenib and the serious adverse reactions caused by this drug, the overall therapeutic effect of HCC is far from satisfactory[4,5]. Thus, it is imperative to explore new drugs for better treatment of HCC.

HYD-PEP06 is an RGD-modified endostatin-derived synthetic polypeptide of 30 amino acids. The RGDRGD fragment attached at its N-terminus can specifically bind to different integrins in endothelial cells. HYD-PEP06 is designed and synthesized by our group and it has been demonstrated to exert anti-tumor effects on colorectal carcinoma and oral squamous cell carcinoma[6,7]. However, whether HYD-PEP06 can also suppress HCC progression and metastasis remained untested.

Epithelial mesenchymal transition (EMT) is a critical mechanism for many pathological processes, including tumor invasion and metastasis. During EMT, epithelial cells discard their epithelial properties and acquire the properties of mesenchymal cells in both morphology and biological characteristics[8,9]. Typical EMT malignant tumor cells are characterized by increased migration, invasion, mesenchymal characteristics, along with downregulation of expression of cell adhesion molecules and upregulation of mesenchymal marker genes[10,11]. EMT plays a key role in conferring the metastatic and invasive properties of HCC[12,13]. Several signaling pathways, such as mitogen-activated protein kinase/extracellular regulated protein kinases (MAPK/ERK), nuclear factor kappa-B (NF-κB) and phosphatidylinositol-3-kinase/protein kinase B (PI3K/AKT), are known to regulate EMT[14−16], of which, the PI3K/AKT pathway is of pivotal importance in controlling tumor invasion and metastasis. Moreover, the PI3K/AKT signaling pathway can induce EMT by dual mechanisms: increasing expression of matrix metalloproteinases and transcription factor Snail[17−21].

Cancer stem cells (CSCs) belong to a subgroup of tumor cells which possess self-regeneration capacity, extensive proliferation and high carcinogenic potential and are considered to be responsible for cancer occurrence, development, chemo-resistance, metastasis and recurrence[22]. Additionally, CSCs have been identified in several types of human cancers including HCC[23]. Accumulating evidence suggests that tumor cells acquire CSC-like characteristics through activating EMT[24,25]. It has been proposed that eliminating CSCs may be a more efficient approach for cancer therapy. Indeed, the self-proliferation and expansion of liver CSCs can activate the WNT signaling pathway to enhance tumor aggressiveness and resistance to chemo-therapeutic agents[26,27]. WNT signaling pathway promotes EMT and metastasis, being considered as a significant mediator of HCC metastasis and a marker of poor prognosis as well[28,29].

The aims of the present study are to characterize the effects of HYD-PEP06 on EMT and metastasis of HCC with both *in vitro* and *in vivo* models and to delineate the underlying signaling mechanisms. Our results indicate that HYD-PEP06 is an anti-HCC agent suppressing metastasis and EMT *via* inhibiting the PI3K/AKT and WNT/β-catenin signaling pathways. The findings suggest that HYD-PEP06 might be considered as a novel short-peptide agent for HCC therapy.

2. Materials and methods

2.1. Cell lines, culture conditions and reagents

Human HCC cell line HCCLM3 was purchased from Cell Bank of Type Culture Collection of Chinese Academy of Sciences (Shanghai, China). Human HCC cell line HepG2 and human umbilical vein endothelial cells (HUVEC) were purchased from the American Type Culture Collection (ATCC).

Cells were cultured in Dulbecco's modified Eagle's medium (DMEM; Hyclone, Utah, USA) with 10% fetal bovine serum (FBS) and 1% antibiotic in 5% CO_2 cell incubator at 37 °C. HYD-PEP06 (RGDRGDMHSHRDFQPVLHLVALQSPLSGGM) was synthesized by Shengnuo Tech Co., Ltd. (Chengdu, China). HYD-PEP06 was dissolved in 5% glucose solution (GS) and filtered. 5-Fluorouracil (5-Fu) was obtained from Tianjin Jinyao Amino Acid Co., Ltd. (Tianjin, China).

2.2. Evaluation of cell viability by CCK8 assay

Cell Counting Kit-8 (CCK-8, MCE, USA) assay was used to evaluate cell viability. HCCLM3 and HepG2 cells (5×10^3/well) were plated into 96-well plates. After the cells had reached 80% confluence, they were starved for 6 h and incubated with different concentrations of HYD-PEP06 for 24 and 48 h. After drug treatment, 10 μL CCK8 was added to each well of the 96-well plate and incubated for 1.5 h. Then the absorbance value was measured at 450 nm by using PowerWave HT microplate spectrophotometer (BioTek, USA). The data of each group was normalized to that of the control group.

2.3. In vitro cell migration assay

Wound healing and Transwell assays were conducted to evaluate tumor cell migration *in vitro*. For wound healing, HCCLM3 and

HepG2 cells (5×10^5/mL) were planted onto a 6-well plate. Then, the cells were incubated with different concentrations of HYD-PEP06 for 24 h. A dense monolayer of cells was scraped from the 6-well plate, and the floating cells were washed with PBS. GS was used as a negative control. Photographs were obtained with a digital Single Lens Reflex Camera. Cell migration area was analyzed by Image J software. Each measurement was conducted at least five times.

Transwell filter chambers (Costar, Corning, NY, USA) were used for migration analysis. HCCLM3, HepG2 and cancer stem-like cells (5×10^4/well) were planted into upper chambers in basal medium without serum. Then, 600 μL serum was added to the lower chambers. After 24 h culturing, the chambers were covered with methanol for 30 min, followed by staining with 0.1% crystal violet for 20 min. The area of stained cells was photographed under a microscope. For each group, five randomly selected microscopic fields were enumerated and analyzed. Each measurement was conducted in triplicate.

2.4. Western blot analysis

Cells were harvested from cultured flask and lysed in a RIPA lysis buffer (Solarbio, China) containing protease and phosphatase inhibitors (MCE, USA). Protein concentration was determined using BCA Protein Assay Kit (Beyotime, China). Cell lysates of 100 μg per lane were separated on a 10% Tris-Tricine SDS-PAGE gel and transferred onto nitrocellulose membranes (PALL, Germany) for 90 min. The blotted membranes were blocked with 5% skimmed milk for 1.5 h and then incubated with primary antibodies at 4 °C overnight. The antibodies against E-cadherin (#14472), N-cadherin (#13116), Vimentin (#5741), phospho-AKT (#4060), pan-AKT (#4691), β-catenin (#8480), Axin2 (#2151), phospho-GSK-3β (#5558), and GSK-3β (#9832) were purchased from Cell Signaling Technology (Boston, MA, USA). The antibodies against α-catenin (ab52227, Abcam, Cambridge, UK), CD133 (WL02586, Wanlei, China), CD44 (WL03531, Wanlei, China) and GAPDH (1E6D9, Protein tech) were used. AKT inhibitor MK2206 (MCE, USA) and activator SC79 (MCE, USA) were obtained from Med Chem Express (Monmouth Junction, NJ, USA). The blotted membranes were scanned by Odyssey Infrared Imaging System (Li-COR, USA) after incubation with secondary antibody. Band densitometry was quantified by using Image J software, and the values were normalized to GAPDH as an internal control.

2.5. Immunofluorescence (IF) assay

IF staining was conducted to analyze the effects of HYD-PEP06 on EMT and cancer stem-like cells. HCCLM3, HepG2 and cancer stem-like cells were seeded on the sterile coverslips laid on 24-well plate, incubated with HYD-PEP06 at 200 μg/mL for 24 h, and then fixed in 4% PFA for 10 min followed by penetration with 0.5% Triton X-100 (Leagene, China) for 15 min and subsequent blocking with goat serum for 1 h. Next, the cells were incubated with primary antibodies against E-cadherin, vimentin, β-catenin or GSK-3β at 4 °C overnight. CD133 (AF5120, Affinity Biosciences, China) and CD44 (DF6392, Affinity Biosciences, China) were used to identify and verify cancer stem-like cells. Then, the cells were incubated with secondary antibody, Alexa Fluor 488 or Alexa Fluor 594 (Invitrogen Thermo Fisher, USA) for 1 h. Cell nuclei were stained with 4,6-diamidino-2-phenylindole (DAPI) at room temperature for 20 min. Finally, images were obtained under a fluorescence microscope (Zeiss, Jena, Germany). All measurements were performed in triplicate.

2.6. Cignal finder pathway reporter array

Cignal Finder Reporter Array (Qiagen, Dusseldorf, Germany) was carried out to investigate the signaling pathways mediating the effects of HYD-PEP06 in HCCLM3 cells and cancer stem-like cells. Briefly, adherent cells (1×10^5/well) were digested from logarithmic growth phase in 96-well plates for 16 h. The cells were transfected with transcription factor responsive reporter constructs of different signaling pathways. Next, the culture medium was replaced by the fresh medium supplemented with 0.5% FBS and 1% antibiotics. After 24 h, 200 μg/mL HYD-PEP06 was added into 96-well plates.

To study the effect of HYD-PEP06 on HCC, luciferase assay was performed by using the Dual-Luciferase Reporter Assay System (Promega, WI, USA) following the instruction handbook. Firstly, a volume of 100 μL Dual-Glo Reagent was added to each well of the 96-well plate after it was removed from the incubator. Waiting for at least 10 min, cell lysis was allowed to occur. Then the firefly luminescence was measured in a luminometer. After that, a volume of 100 μL Dual-Glo Stop & Glo Reagent was added. Waiting for at least another 10 min, *Renilla* luminescence was measured and the luminescence ratio of HYD-PEP06 group to the control group was calculated. Finally, relative response ratios were calculated from the normalized ratios.

2.7. Tube network formation

Tube formation assay was conducted in Matrigel for assessing angiogenesis *in vitro*. The 24-well plate was covered with growth-factor reduced Matrigel (250 μL/well) under cooling condition and incubated for coagulation at 37 °C for 30 min. Serum starved HUVEC cells (1.5×10^5/mL) were resuspended in Endothelial Basal Medium-2 supplemented with 0.5% FBS or in tumor stem cell enrichment medium, and then seeded onto Matrigel-coated well after incubation with 200 μg/mL HYD-PEP06 for 8 h. Next, the morphological changes of the tube formation were imaged in multiple fields per well under a microscope (Olympus, Tokyo, Japan). Mean capillary tube length and the number of branching nodes were quantified by Image J software at three random fields for 5 times.

2.8. Culture and isolation of hepatocellular cancer stem-like cells

HepG2 cells were cultured with DMEM medium containing 10% FBS, 1% penicillin and streptomycin in 5% CO_2 at 37 °C. At the logarithmic growth phase, the cells were trypsinization collected by centrifugation and resuspended in FBS-free CSC culture medium Dulbecco's modified Eagle's medium/Nutrient Mixture F-12 (DMEM/F12, Hyclone, UT, USA) containing 20 ng/mL basic fibroblast growth factor, 20 ng/mL epidermal growth factor (PeproTech, Rocky Hill, NJ, USA), 4 μg/mL heparin sodium, 20 μL/mL B27 serum substitute supplement, and 1% antibiotic. Then the cells were seeded into polyhydroxy ethyl meth-acrylate pretreatment cell culture flask for two weeks. The adherent cells were discarded. Then the suspending cells were collected and cultured in stem cell culture medium. Cell digestion and passage were conducted every 10 days, the sphere formation was observed under the microscope every 3 days. The cells without the efficient

sphere-forming capacity deposited at the bottom of ultra-low attachment surface plates were discard carefully, sphere-like cells were collected for further use when spheroids reached a diameter of 100 μm in about 2 weeks.

2.9. Formation and proliferation of 3D spheroids

Cancer stem-like cells (1×10^4/well) were planted onto Ultra-low adhesion 96-well plates (S-BIO, New Hampshire, USA). Three-dimensional (3D) spheroids were photographed every 24 h, and sphere area was measured with Image J software. To evaluate 3D spheroid proliferation in the presence of HYD-PEP06, the photographs were taken under a microscope (Olympus, Tokyo, Japan) and analyzed using Image J software.

2.10. Postsurgical residual tumor xenograft models and anti-tumor effect assay

Adult female 6−8 weeks old athymic BALB/c *nu/nu* nude mice (15−20 g) were obtained from Beijing Vital River Laboratory Animal Technology Co., Ltd. [Certificate No. SCXK(Jing) 2016-0006]. The animals were raised in a constant temperature of 23 ± 2 °C under a 12 h day and night cycle by feeding with sterilized food and sterile water. A mouse model of postsurgical residual tumor was used to imitate the recurrence of solid tumor, and HCCLM3 cells were digested and collected. First, a traditional tumor xenograft nude mouse model was established by injecting 200 μL 1×10^6/mL HCCLM3 cell suspension subcutaneously into the right axillary of mice. Once the average volume of tumors had reached 1000−1500 mm^3, they were aseptically removed from the mice and cut into small pieces. Then, the tumor chunks were subcutaneously inoculated to the tumor xenograft nude mice. After the average volume of the tumors had reached to 300−350 mm^3, the mice were intravenously injected 1.2% avertin solution for anesthetization. Residual tumor model of average volume 60−100 mm^3 was aseptically constructed by removing parts of tumors. After 24 h, mice were categorized into four groups ($n = 10$) based on tumor volume, which included the control groups, a low concentration of 5 mg/kg HYD-PEP06, a medium concentration of 10 mg/kg HYD-PEP06 and a high concentration of 20 mg/kg HYD-PEP06. Each group was daily injected with either GS or HYD-PEP06 intravenously for 14 days. The width and length of tumors were calculated by caliper every other day. Tumor volume was calculated on the basic of the width and length of tumors. On Day 14 after injection of HYD-PEP06, the groups were euthanized. Then the tumors were cut, weighted, and immersed in 4% paraformaldehyde at 37 °C for Western blot analysis. The tumor volume inhibitory rate was calculated according to Eq. (1):

$$\mathrm{IR}(\%) = (V_t - V_0) / V_0 \times 100 \quad (1)$$

where V_0 presents the control tumor volume and V_t is the HYD-PEP06 groups tumor volume. The tumor weight inhibitory rate was calculated according to Eq. (2):

$$\mathrm{IR}(\%) = (W_t - W_0) / W_t \times 100 \quad (2)$$

where W_t and W_0 presented the tumor weights of the HYD-PEP06 groups and control groups.

The protocols for animal experiments were approved by the Institution Animal Care and Use Committee of Harbin Medical University (Harbin, China), and the procedures conformed to the Guide for the Care and Use of Laboratory Animals, and exactly following with the People's Republic of China Legislation Regarding the Use and Care of Laboratory Animals.

2.11. Mouse model of hepatocellular cancer pulmonary metastasis

Adult female 4 weeks old athymic BALB/c *nu/nu* nude mice (15−20 g) were purchased from Beijing Vital River Laboratory Animal Technology Co., Ltd. [Certificate No. SCXK (Jing) 2016-0011 (No.11400700230989)]. The animals were raised in a controlled aseptic environment as described above.

HCCLM3 cells were cultured in DMEM medium (Hyclone, Utah, USA) added with 10% FBS and 1% antibotic at 37 °C in 5% CO_2. HCCLM3 cells were transfected by self-inactivated lentiviral vector pCDH-luc2-GFP, then added 1 μg/mL puromycin (ThermoFisher Scientific, MA, USA) to the medium to establish a cell line which stably expressed luciferase 2 and green fluorescent protein (HCCLM3-Luc2-GFP). A total of 1.5×10^6 stable expression vector cells suspension in 200 μL saline were gently injected through tail vein. After 5 min the anaesthetized mice were intraperitoneal injection with 150 mg/kg D-luciferin, and imaged by IVIS Spectrum CT platform (Pekin Elmer, MA, USA). Data was analyzed by living image 4.3.1 software. The percentage of tumor growth was calculated according to Eq. (3):

$$\begin{aligned}\text{Tumor growth}(\%) = &(\text{Total flux of photons of the control group} \\ &- \text{Total flux of photons of HYD} - \text{PEP06 group}) / \text{Total flux} \\ &\text{of photons of the control groups} \times 100 \end{aligned} \quad (3)$$

To test HYD-PEP06 on the efficacy of the HCC tumor pulmonary metastasis model, mice were randomly categorized into four groups after injecting HCCLM3 tumor cells 5 min ago. Based on the bioluminescence imaging (BLI) signals, the mice ($n = 40$) were categorized into four groups: control group, 5 mg/kg, 10 mg/kg and 20 mg/kg HYD-PEP06-treated groups. Each group was daily administered with either GS or HYD-PEP06 by intravenous injection for 28 days. The mice were euthanized on the last day and then the main internal organs were collected for BLI imaging *in vitro* which included brain, stomach, lung, heart, colon, kidney, spleen and small intestine.

2.12. Statistical analysis

Data are presented as mean ± standard error of mean (SEM) for three independent experiments. One-way ANOVA followed by the Tukey procedure was used by comparing the mean values in multiple groups. $P < 0.05$ indicates statistical significance. Statistical significances between two groups were performed with Student *t*-test. Kaplan−Meier technique was performed to plot survival curves. Results were performed for three times. Statistical analysis was conducted by Prism 7.0c GraphPad Software (GraphPad; San Diego, CA, USA).

3. Results

3.1. HYD-PEP06 inhibits hepatocellular carcinoma metastasis *in vitro*

The mechanism for anti-tumor drugs can be various, including killing dividing cancer cells, suppressing cell proliferation and blocking the spread of cancer cells[30,31]. To investigate the effect

of HYD-PEP06 on cancer cells, CCK8 assay was used to assess the viability of HCCLM3 and HepG2 cell lines. There were no significant differences of the cell viability after treatment with either glucose or HYD-PEP06 at concentrations from 12.5 to 400 μg/mL. In contrast, the viability of HCCLM3 and HepG2 cells was significantly reduced by 5-fluorouracil (5-FU, Fig. 1A−D).

Next, wound-healing and Transwell migration assays were performed to investigate the effects of HYD-PEP06 on metastasis of HCC. As depicted in Fig. 2A and B, treatment of different concentrations of HYD-PEP06 (50, 100 and 200 μg/mL) for 24 h inhibited the migration of both HCCLM3 and HepG2 cells in a dose-dependent fashion ($P < 0.001$, Fig. 2C). Similar results were observed with the Transwell migration assay: HYD-PEP06 (200 μg/mL) reduced the migration of HCCLM3 and HepG2 cells by 72.1% and 82.1%, respectively (Fig. 2D and E). These data suggest that HYD-PEP06 inhibits metastasis without affecting viability in HCC.

3.2. *HYD-PEP06 suppresses HCC metastasis by inhibiting epithelial mesenchymal (EMT) transition in HCC cells*

It is known that EMT enables non-metastatic tumor cells to infiltrate into surrounding tissues and eventually metastasizes to distant sites[9]. In this process, cells change from their epithelial "cobblestone" phenotype to the spindle-shaped morphological characteristics of mesenchymal cells, causing enhanced motility and invasion[32,33]. Western blot results show that the expression of epithelial markers E-cadherin and α-catenin was significantly increased, along with concomitant downregulation of mesenchymal markers N-cadherin and vimentin after HYD-PEP06 treatment in HCCLM3 (Fig. 3A−E). Similar results were found in HepG2 cells (Fig. 3F−J). In addition, immunofluorescent staining demonstrated that vimentin expression was significantly decreased by HYD-PEP06 (200 μg/mL) treatment for 24 h, whereas E-cadherin expression was increased (Fig. 3K and L).

3.3. *HYD-PEP06 inhibits tumor metastasis and EMT in human HCC by blocking the PI3K/AKT pathway*

To decipher the mechanisms by which HYD-PEP06 suppresses HCC metastasis and EMT, we conducted the Cignal Finder Reporter Arrays for the comprehensive analysis of 10 signaling pathways to pinpoint the pathways perturbed by 200 μg/mL HYD-PEP06 in HCCLM3 cells after 24 h treatment. Using a cut-off fold change >1.5 and *P*-value ≤0.05 criteria, we identified the PI3K/AKT reporter gene to be a negatively regulated signaling pathway (reduced by approximately 4-fold, Fig. 4A). Moreover, Western blot results reveal that HYD-PEP06 significantly decreased the protein level of active or phosphorylated AKT (p-AKT) in HCCLM3 cells without altering the total AKT protein level (Fig. 4B and C). Furthermore, HYD-PEP06 substantially inhibited the phosphorylation of AKT after adding to AKT inhibitor MK2206 (10 μmol/L). Meanwhile, MK2206 exacerbated the effects of HYD-PEP06 in greater

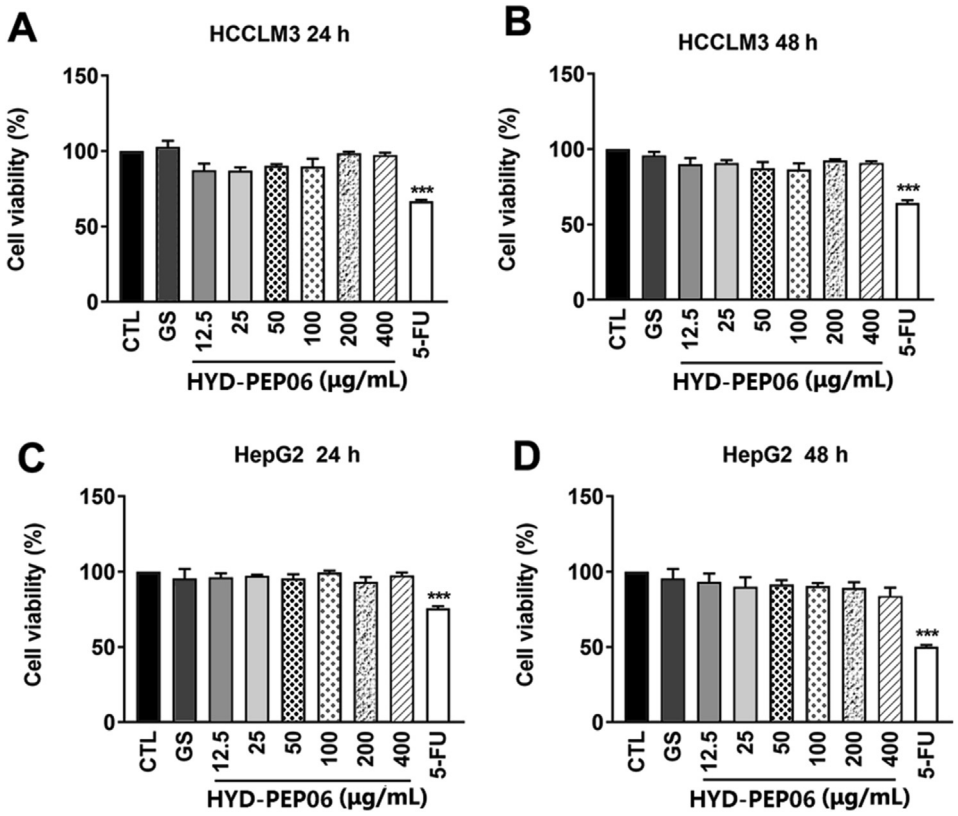

Figure 1 HYD-PEP06 does not affect cell viability of HCCLM3 and HepG2 cells. (A)−(D) HCCLM3 and HepG2 cells were treated with various concentrations of HYD-PEP06 (12.5, 25, 50, 100, 200 and 400 μg/mL) for 24 or 48 h, and cell viability was determined by Cell Counting Kit-8 (CCK8) assay. Glucose solution (GS) was used as a solvent control and 5-fluorouracil (5-FU) as a positive control. Data were calculated from three independent experiments and are presented as mean ± SEM; ***$P < 0.001$ by one-way ANOVA followed by Tukey's test.

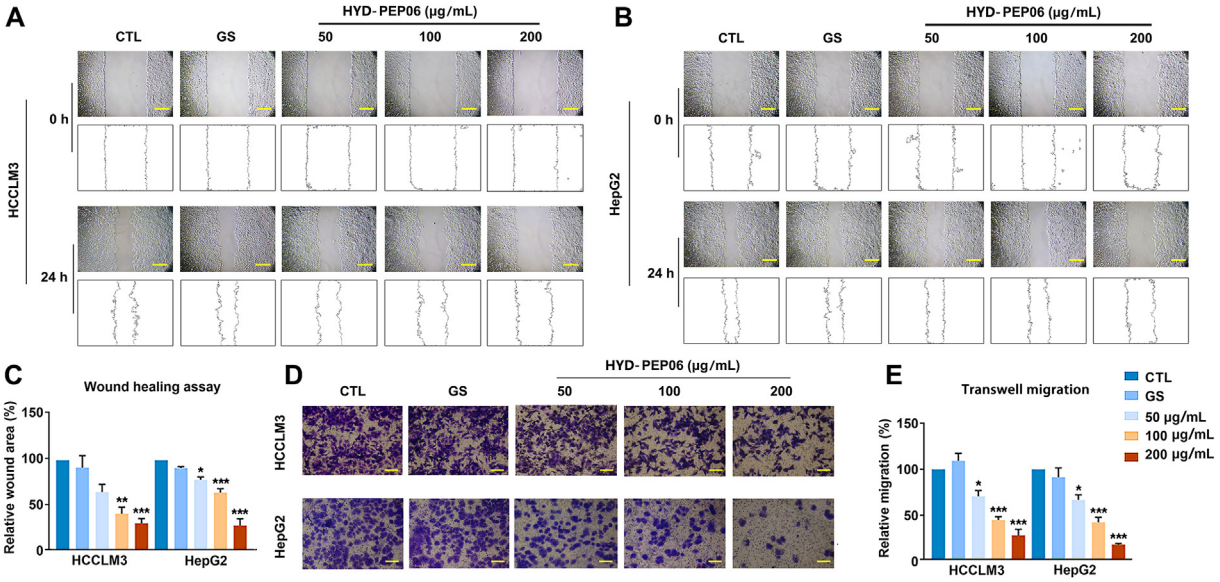

Figure 2 Inhibitory effects of HYD-PEP06 on the migration potential in hepatocellular carcinoma cells HCCLM3 and HepG2. HYD-PEP06 dramatically suppressed the metastasis of (A) HCCLM3 and (B) HepG2 cells in wound healing assay. Magnification: 400 ×. (C) The wound healing results show the concentration-dependent inhibition of metastasis by HYD-PEP06. Data are expressed as mean ± SEM; $*P < 0.05$, $**P < 0.01$, $***P < 0.001$ *vs*. Control. (D) Migration of HCCLM3 and HepG2 cells was decreased by HYD-PEP06 in Transwell assay. Scale bar: 100 μm. Five independent experiments were examined, and representative images are presented here. (E) Transwell assay shows the concentration-dependent inhibitory effect of HYD-PEP06 on migration. The data are expressed as mean ± SEM; $*P < 0.05$, $***P < 0.001$ *vs*. Control.

downregulation of vimentin and N-cadherin protein expression, along with greater up-regulation of α-cadherin and E-cadherin protein expression in HCCLM3 cells (Fig. 4D−I). Conversely, SC79 (an AKT activator) reversed the downregulation of the mesenchymal markers and upregulation of the epithelial markers induced by HYD-PEP06 (Fig. 4J−O).

3.4. HYD-PEP06 attenuates the metastatic potential of cancer stem-like cells isolated from HepG2 cells

Cancer stem cells (CSCs) contribute to HCC metastasis, progression and recurrence after therapy, by inducing EMT[34−37]. We therefore continued to investigate whether HYD-PEP06 has any effects on CSCs. Our study reveals that HepG2 cells expressed higher levels of CSC markers CD133 and CD44 than HCCLM3 cells (Fig. 5A−C), suggesting that the former possesses high-stemness ability than the latter. Thus, we isolated stem-like cells from HepG2 cells for the subsequent experiments. Cancer 3D spheroid culture is a widely used model for studying CSCs[38]. In the medium with serum, HepG2 cells were polygonal morphology. The tumor spheres were obtained from HepG2 cells, which suspended in FBS-free DMEM/F12. Cells cultured for 10 days demonstrated round shape with few cells exhibiting epithelial-like morphology. We observed the size of the sphere under the microscope on Days 0, 3, 5, 7 and 10. HepG2 cells with stem-like properties have efficient sphere-forming capacity under serum-free conditions, and three-dimensional (3D) spheres growth over time (Fig. 5D). Cells without the efficient sphere-forming capacity deposited at the bottom of ultra-low attachment surface plates were discard carefully. When the suspension of spheres reached a diameter of 100 μm, the sphere-forming efficiency was calculated. And spheres were collected for further experiments. CSC population in solid tumors is identified by typical markers such as CD133/CD44 and characterized by high tumorigenicity and invasiveness[38]. The isolated stem-like cells expressed higher protein levels of both CD133 and CD44 than HepG2 cells, as determined by Western blot analysis (Fig. 5E−G) and immunofluorescence staining (Fig. 5H). Moreover, while HepG2 cells formed smaller tumors in mouse xenograft model, the isolated tumor spheres xenotransplants generated impressively larger tumors (Fig. 5I). The xenograft tumors derived from HepG2 cells and the isolated CSCs were harvested two weeks after subcutaneous inoculation in nude mice. The Western blot results demonstrate that the xenograft tumors derived from CSCs expressing higher levels of CD133 and CD44 than those derived from HepG2 cells (Fig. 5J−L).

Moreover, 3D spheroids formation assay demonstrated treatment of HYD-PEP06 for 24 and 48 h inhibited the formation of 3D tumor spheroids compared with control or glucose solution (GS) group, indicating inhibitory effect of the polypeptide 30 on cancer stemness (Fig. 6A and B). In addition, Transwell assay exhibited remarkable reduction of CSCs migration in the presence of HYD-PEP06 (Fig. 6C and D). Furthermore, the effects of HYD-PEP06 on tube formation were evaluated in HUVEC cells. The culture medium collected from CSCs was more favorable to form tube formation relative to that of regular HepG2 cells, as indicated by more dense meshwork of branching capillary-like tubules formed by connection between neighboring cells (Fig. 6E−G). Strikingly, the intercellular tube formation was considerably abrogated by HYD-PEP06 as HUVEC cells being failed to form tubes and essentially staying as separate spherical bodies. These findings indicate that HYD-

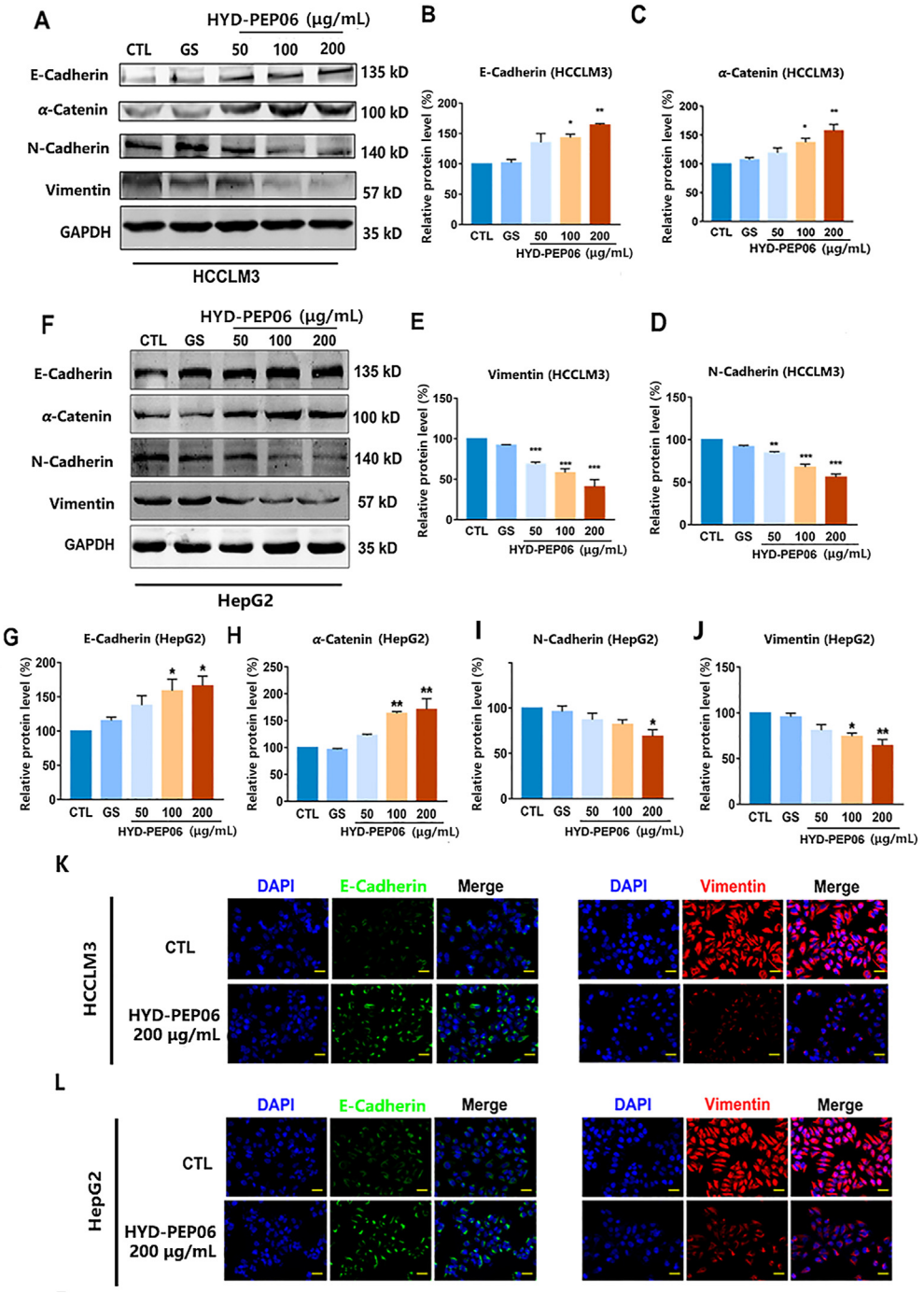

Figure 3 HYD-PEP06 inhibits the transition between epithelial and mesenchymal phenotypes in HCC cells. (A) Western blot results illustrating the effects of HYD-PEP06 (50, 100, and 200 μg/mL) for 24 h on the protein expression of the epithelial and mesenchymal markers in HCCLM3 cells. (B)−(E) HYD-PEP06 increased the levels of epithelial marker proteins and decreased the levels of mesenchymal marker proteins in HCCLM3 cells compared with control. (F) Western blot data demonstrating the effects of HYD-PEP06 (50, 100, and 200 μg/mL) for 24 h on the protein expression of the epithelial and mesenchymal markers in HepG2 cells. (G)−(J) HYD-PEP06 increased the epithelial markers protein levels and decreased the mesenchymal markers protein levels in HepG2 cells compared with control. Data are expressed as mean ± SEM; $^{*}P < 0.05$, $^{**}P < 0.01$, $^{***}P < 0.001$, compared with Control. (K) and (L) Effects of HYD-PEP06 (200 μg/mL) on the expression of the classical epithelial and mesenchymal markers were evaluated by immunofluorescence assay. Blue represents 4′,6-diamidino-2-phenylindole (DAPI) for nucleus; green represents E-cadherin; red represents vimentin. Magnification: 400 ×.

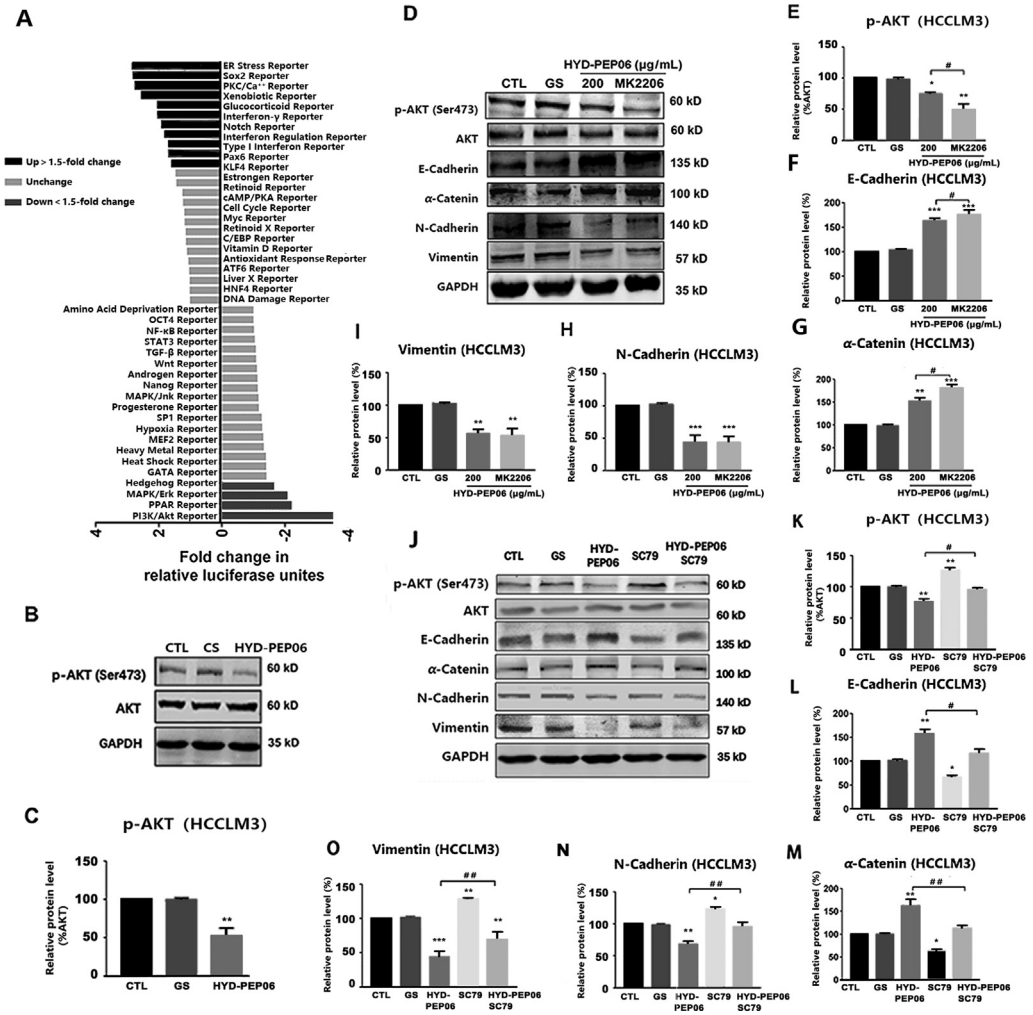

Figure 4 HYD-PEP06 attenuated EMT phenotype in HCCLM3 though inhibiting PI3K/AKT signaling pathway. (A) The levels of transcription activities of HYD-PEP06 (200 μg/mL) treated or untreated HCCLM3 cells by Cignal Finder Reporter Pathway Arrays. PI3K/AKT signaling was significantly downregulated in HCCLM3 cells after HYD-PEP06 treatment for 24 h, while other signaling pathways indicated no significant difference. (B) Western blot results of p-AKT and AKT expression levels after adding 200 μg/mL HYD-PEP06 to HCCLM3 cells for 24 h. (C) The densitometry of p-AKT and AKT proteins assessed by Western blot analysis. (D) HCCLM3 cells were pretreated with or without 10 μmol/L MK2206 (a PI3K/AKT inhibitor) and then with HYD-PEP06 (200 μg/mL) for 24 h. The protein expression of p-AKT, AKT, the epithelial and mesenchymal markers was determined by Western blot. (E)−(I) The protein expression of p-AKT, AKT, the epithelial and mesenchymal markers was assessed by adding the AKT inhibitor MK2206 (10 μmol/L). (J) HCCLM3 cells were pretreated with or without 10 μmol/L SC79 (a PI3K/AKT agonist) and then with or without HYD-PEP06 (200 μg/mL) for 24 h. The protein expression of p-AKT, AKT, the epithelial and mesenchymal markers were semi-quantified by Western blot. (K)−(O) The protein levels of p-AKT, AKT, the epithelial and mesenchymal markers were examined in the presence of an AKT agonist SC79 (10 μmol/L). All the Western blot data are presented as mean ± SEM; $^{*}P < 0.05$, $^{**}P < 0.01$, $^{***}P < 0.001$ *vs*. Control; $^{\#}P < 0.05$, $^{\#\#}P < 0.01$ *vs*. HYD-PEP06 (200 μg/mL).

PEP06 suppresses the angiogenesis by manipulating CSC-like cells.

3.5. HYD-PEP06 inhibits the metastatic potential of CSC-like cells by suppressing the canonical WNT/β-catenin pathway

To investigate the mechanisms by which HYD-PEP06 suppresses the metastatic potential of CSCs, we conducted the Cignal Finder Reporter Arrays. As illustrated in Fig. 7A, WNT was substantially down-regulated in CSC-like cells after treatment with 200 μg/mL HYD-PEP06 for 24 h. We therefore hypothesized that HYD-PEP06 might attenuate CSC metastasis *via* the WNT/β-catenin pathway. To test this notion, we measured the protein levels of β-catenin, axin2, p-GSK-3β and total GSK-3β, the mediators of the WNT/β-catenin signaling pathway. As illustrated in Fig. 7B−E, HYD-PEP06 significantly downregulated the expression of β-catenin, axin2, and p-GSK-3β in CSC-like cells. Considering that accumulated β-catenin can be translocated to the nucleus, we conducted immunofluorescent staining to analyze the expression and subcellular distribution of β-catenin in the presence of HYD-PEP06. As expected, CSC-like cells in control group exhibited even distributions of β-catenin in cytoplasm and nucleus, whereas in the presence of HYD-PEP06, β-catenin appeared more restricted to the localization close to cytoplasmic membrane while nuclear β-catenin protein substantially decreased (Fig. 7F). The level of total GSK-3β protein didn't change after HYD-PEP06

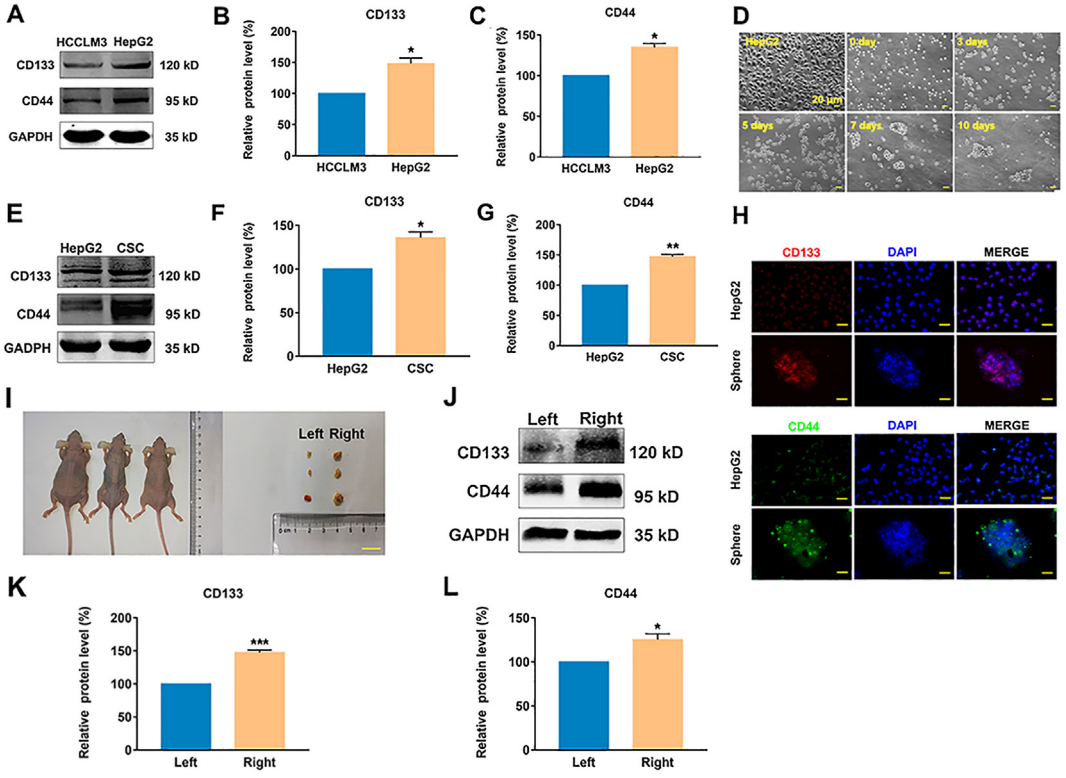

Figure 5 Tumor spheres isolated from hepatocellular carcinoma HepG2 cells obtained the characteristics of cancer stem cells. (A) Comparison of the protein levels of CD133 and CD44 in HCCLM3 and HepG2 cells. The protein expression of (B) CD133 and (C) CD44 was dramatically increased in HepG2 cells compared with those in HCCLM3 cells. $^{*}P < 0.05$, compared with the HCCLM3 cells. (D) The images of 3D tumor spheroids were captured using the fluorescence microscope on Day 0 in attachment surface plates and Days 0, 3, 5, 7, and 10 in ultra-low attachment surface plates with CSC medium (magnification 200 ×); scale bar: 20 μm. (E) The protein expression of CD133 and CD44 was analyzed by Western blot in HepG2 and CSC-like cells. The protein expression of (F) CD133 and (G) CD44 was dramatically increased in CSC-like cells compared with HepG2 cells. Data are presented as mean ± SEM; $^{*}P < 0.05$, $^{**}P < 0.01$. (H) The expression of CD133 and CD44 were assessed by immunofluorescence staining in HepG2 and tumor sphere cells. Blue represents DAPI; green represents CD44; red represents CD133. Magnification: 400 ×. (I) CSC augments tumor-initiating *in vivo*. Representative xenograft tumors derived from CSC-like cells compared to HepG2 cells after two weeks subcutaneous injection in nude mice ($n = 3$). Left panel: HepG2 cells; right: CSCs. (J) The protein levels of CD133 and CD44 were analyzed by Western blot in the tumor tissues isolated from xenograft models. GAPDH served as a sample loading control. The protein levels of CSC markers (K) CD133 and (L) CD44 were dramatically upregulated in right tissues compared with left tissues. Data are presented as mean ± SEM; $^{*}P < 0.05$, $^{***}P < 0.001$.

treatment (Fig. 7G). These results suggest that the anti-metastasis effect of HYD-PEP06 in CSC-like cells might be attributable to its ability to regulate the canonical WNT/β-catenin pathway.

3.6. HYD-PEP06 suppresses HCC tumor growth in a postsurgical residual tumor xenograft model

Recurrence caused by metastatic spreads from the primary tumor usually peaks in the first two years after tumor resection and carries a poor prognosis[39]. Additionally, surgical resection may promote the growth of residual tumor. Therefore, a mouse model of postoperative recurrent tumor was constructed to assess the effect of HYD-PEP06 on tumor suppression. Clinical post-operative recurrence model was mimicked by surgically excising a part of the primary HCC tumors with a section of 60 mm^3 tumor tissue. The average tumor width, length and body weights were measured every 2−3 days. Administration of different dosages of HYD-PEP06 (5, 10, and 20 mg/kg) through tail vein injection significantly suppressed HCC tumor growth in xenograft mice, as reported by substantial decrease of residue tumor growth compared with the control group (Fig. 8A−D). Specifically, HYD-PEP06 at 5, 10 and 20 mg/kg resulted in 18.0%, 24.1% and 31.4% decreases in tumor weight, respectively. Consistently, HYD-PEP06 caused dose-dependent reduction of HCC tumor volume (20.59%, 31.17%, and 39.18%, respectively; Table 1). Moreover, the anti-tumor effect of HYD-PEP06 was also supported by a slower increase of the tumor volume. The body weight of the mice was unaffected by the peptide (Fig. 8E). Consistent with the above results, Western blot results indicate that the epithelial protein markers were upregulated while the mesenchymal protein markers were downregulated in the tumor specimens from mice treated with HYD-PEP06 relative to the control group (Fig. 8F−J).

3.7. HYD-PEP06 inhibited pulmonary metastasis of HCC in a mice model

To evaluate the efficacy of HYD-PEP06 in inhibiting the metastasis potential of HCC *in vivo*, the metastatic tumor growth in a mouse model of HCC was investigated by bioluminescence imaging. The accumulation of GFP-Luc2-transfected HCCLM3 cells

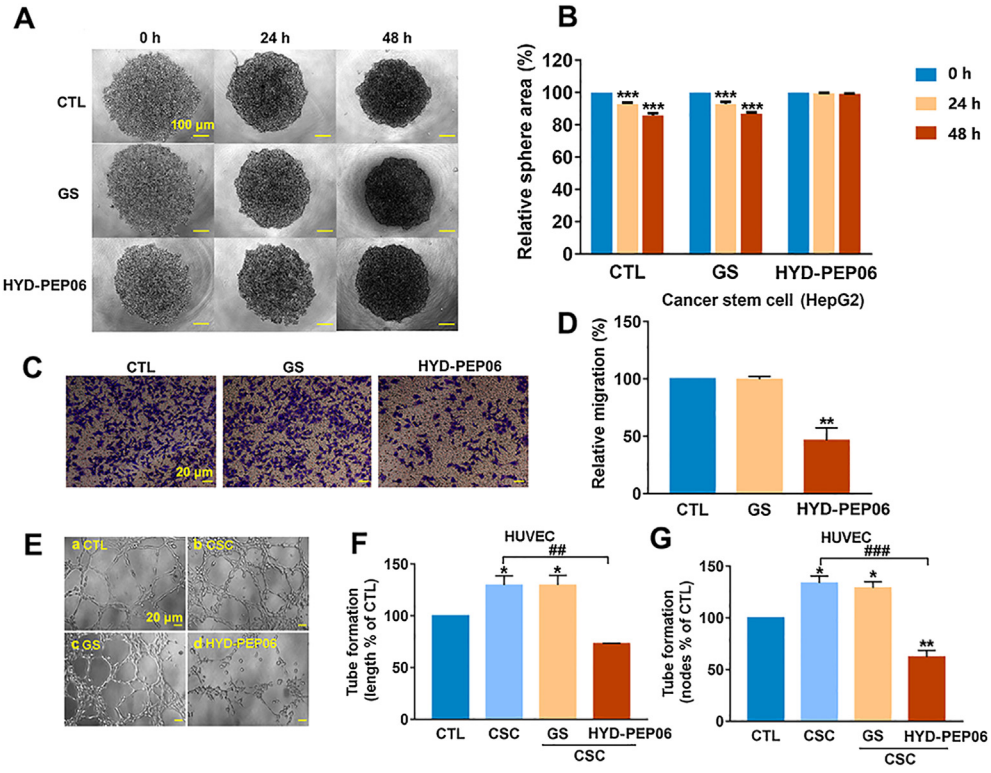

Figure 6 HYD-PEP06 restricted CSC migration behaviors in the CSC isolated from HepG2 cells. (A) Inhibitory efficacy of HYD-PEP06 on migration of 3D tumor spheroids after 24 and 48 h. The cell imaging was performed using the fluorescence microscope every 24 h (magnification 80 ×); scale bar: 100 μm. (B) HYD-PEP06 has no significant effect on the area of the tumor sphere compared with control. Data are presented as mean ± SEM; $^{***}P < 0.001$. (C) and (D) Representative images and the number of migration cells in the CSCs. Data are presented as mean ± SEM; $^{**}P < 0.01$ compared with control. (E)−(G) Typical diagrams and quantitative analysis of capillary tubes formation in HUVECs followed by treating with conditioned medium obtained from the CSCs and HYD-PEP06 (200 μg/mL). Data are presented as mean ± SEM; $^{*}P < 0.05$, $^{**}P < 0.01$ *vs*. control; $^{\#\#}P < 0.01$, $^{\#\#\#}P < 0.001$ *vs*. the CSC group.

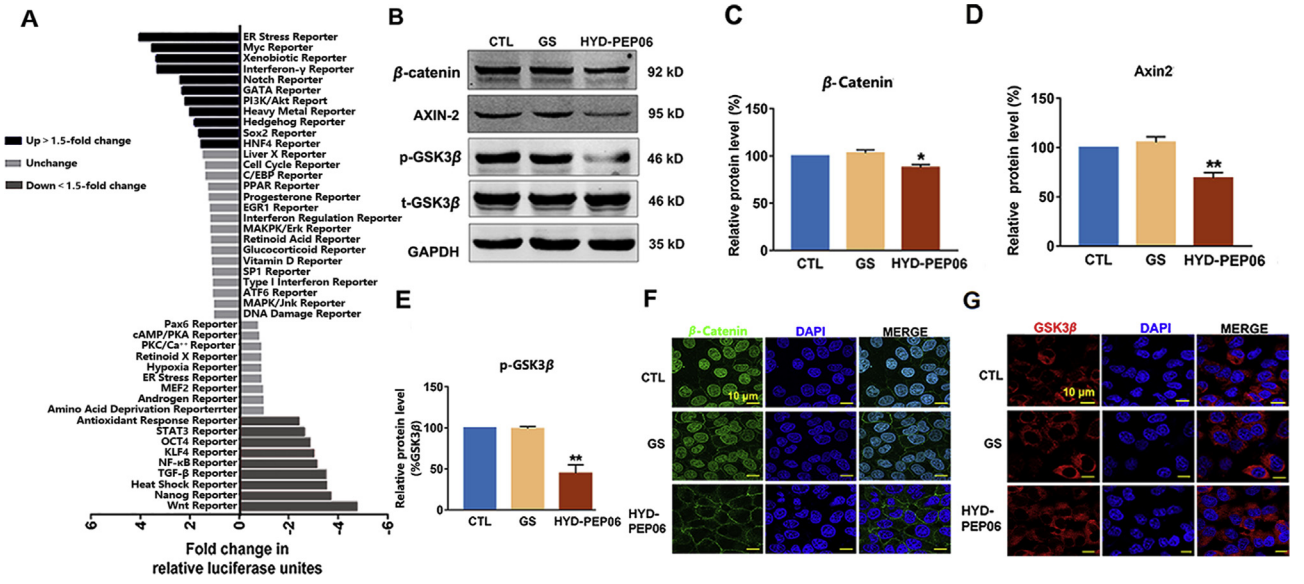

Figure 7 HYD-PEP06 inhibited migration of CSC-like cells *via* downregulating WNT/β-catenin signaling pathway. (A) Differential expression of genes in HYD-PEP06 (200 μg/mL)-treated CSCs and non-treated ones by signal finder reporter pathway array. WNT/β-catenin signaling was significantly downregulated by > 4-fold in CSC after treating HYD-PEP06 (200 μg/mL) for 24 h while the other signaling pathways remained unaltered. (B) HYD-PEP06 (200 μg/mL) inhibited the activation of the WNT/β-catenin signal pathway. The main components/mediators of the WNT/β-catenin signaling pathway were found downregulated at the protein level, including β-catenin, axin2, and p-GSK-3β in CSC-like cells after 24 h HYD-PEP06 treatment, as compared with those in non-treated CSC-like cells. GAPDH act as an internal control. (C)−(E) The averaged Western blot band densities of β-catenin, axin2 and p-GSK-3β proteins. HYD-PEP06 significantly reduced the band densities. $^{*}P < 0.05$, $^{**}P < 0.01$ *vs*. control. (F) and (G) The expression of β-catenin and GSK-3β was assessed by immunofluorescence assay. Blue represents DAPI; green represents β-catenin; red represents GSK-3β. Scale bar: 10 μm.

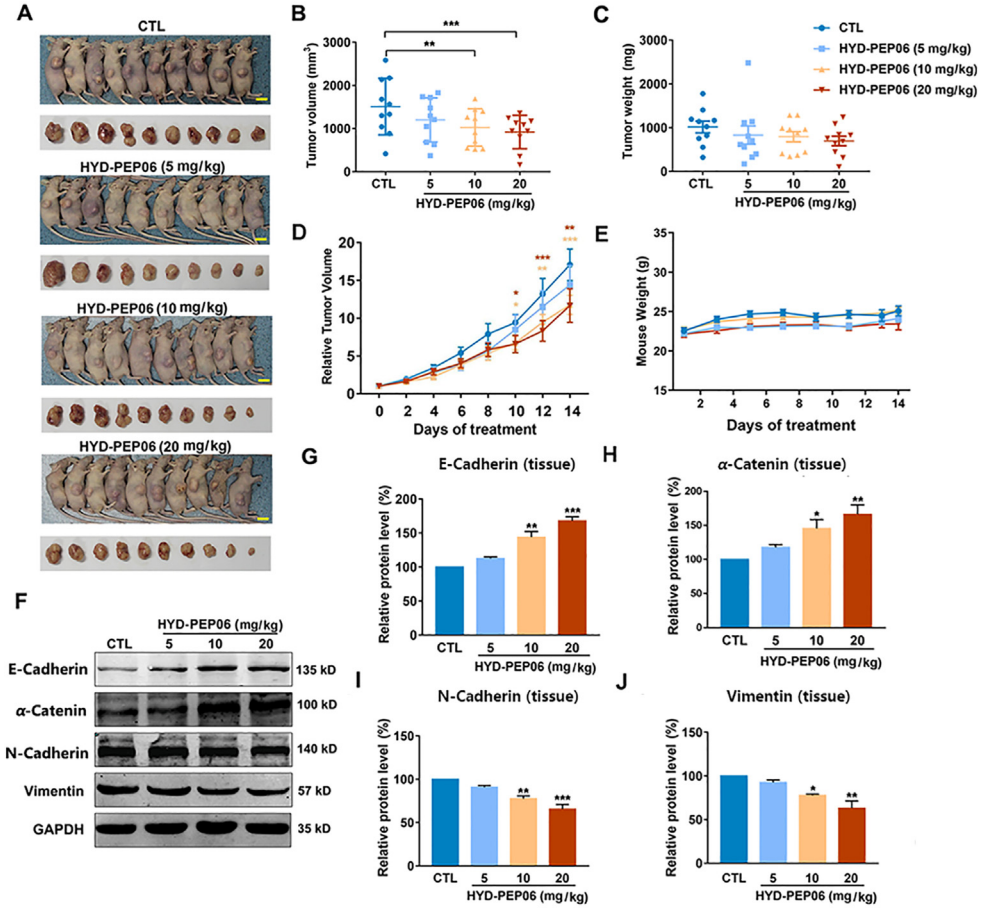

Figure 8 HYD-PEP06 inhibits HCC growth *in vivo*. (A) Images of HCCLM3 residual tumor xenografts treated with GS and HYD-PEP06 (5, 10, and 20 mg/kg). Scale bar: 1 cm. (B) and (C) Tumor growth scatter plots; (D) and (E) curve suggest the inhibitory growth of HCCLM3 residual tumor and the average body weight of the mouse by HYD-PEP06 in a xenograft mouse model. Data are presented as mean ± SEM; $^{*}P < 0.05$, $^{**}P < 0.01$, $^{***}P < 0.001$ *vs*. control by unpaired *t* test. (F) The expression of EMT markers were assessed by Western blot. (G)−(J) Western blot results show that HYD-PEP06 inhibited the expression of the mesenchymal markers, while increasing the levels of the epithelial markers. Data are presented as mean ± SEM; $^{*}P < 0.05$, $^{**}P < 0.01$, $^{***}P < 0.001$ *vs*. control.

in mouse lungs was verified by BLI images after intravenous injection for 5 min. The mice were evenly assigned into four groups ($n = 10$ per group) on the basic of equal mean BLI signal intensities. Most tumor cells were cleared by the immune system of the animals on the first seven days with a loss of BLI signals in all groups. However, the control group showed certain conspicuous bioluminescent signals in the lung on Day 14. Concomitantly, only few mice treated with HYD-PEP06 developed obvious signals. From Days 21−28, HYD-PEP06 dramatically decreased the accumulation of BLI signals in the lung (Fig. 9A and B, and Supporting Information Fig. S1). On the last day (Day 28), the mean BLI signal intensity of the control group was 7.9-fold higher than that on Day 1, while that of the HYD-PEP06 (5, 10 and 20 mg/kg) groups was all markedly lower than on Day 1 (0.31-,

Table 1 Antitumor activity of HYD-PEP06 on postsurgical residual tumor xenografts of human hepatocellular cell in nude mice.

Drug administration		Toxicity		Anticancer activity				
Group	Dose (mg/kg)[a]	Average body weight (g)		Death	Tumor weight (g)	IR (%)	Tumor volume (mm^3)	IR (%)
		Start	Stop					
Control	−	22.55 ± 0.39	25.08 ± 0.63	0/10	1.0153 ± 0.1338	−	1511.89 ± 208.21	−
HYD-PEP06	20	22.03 ± 0.38	22.48 ± 1.15	0/10	0.6962 ± 0.1082	31.44	919.53 ± 122.09**	39.18
HYD-PEP06	10	24.42 ± 0.48	23.60 ± 0.09	0/10	0.7708 ± 0.1086	24.09	1040.61 ± 132.77***	31.17
HYD-PEP06	5	22.19 ± 0.27	24.09 ± 0.44	0/10	0.8323 ± 0.2086	18.02	1200.64 ± 161.54	20.59

The significance of differences (*vs*. control) was determined by one-way ANOVA and Student's *t*-test. Data are presented as mean ± SEM, $n = 10$; $^{**}P < 0.01$, $^{***}P < 0.001$.

[a]QD × 14 days, iv. QD, every day; IR, inhibitory rate; iv represents vein injection daily.

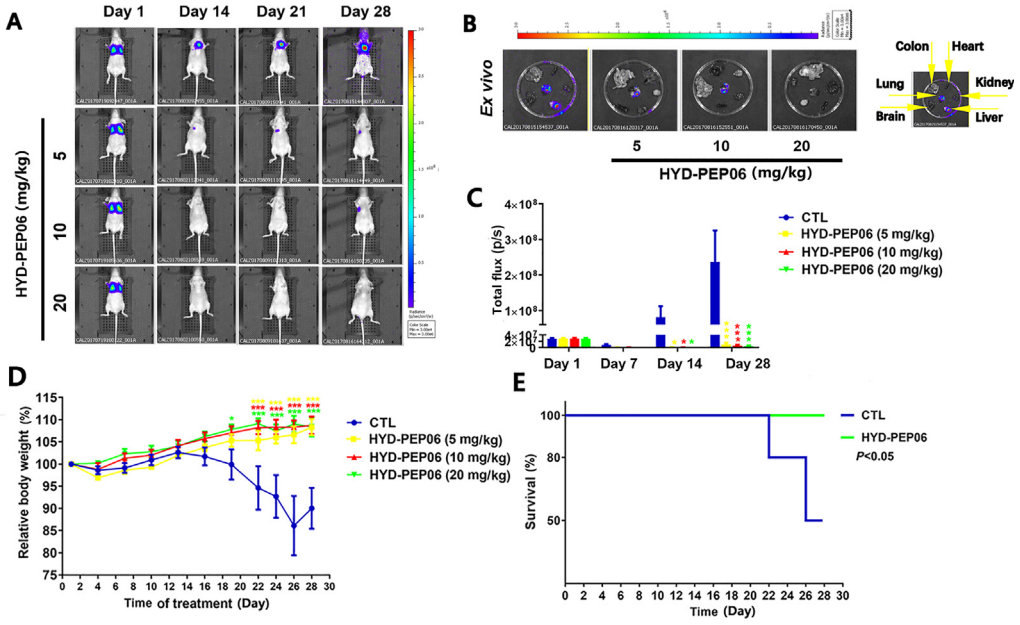

Figure 9 HYD-PEP06 suppresses HCC lung metastasis *in vivo* and increases survival time. (A) Representative BLI of tumor development in mice after injecting GFP-Luc2-transfected HCCLM3 cells after GS and HYD-PEP06 intravenous injection. (B) The statistical graph of the bioluminescent signal intensities. The integrated flux of photons (photons/s) was automatically generated by the Living Image processing software. The lung metastasis of HCCLM3 cells was dramatically suppressed in the HYD-PEP06 group. BLI signals intensities were calculated by the IVIS imaging system. Data are presented as mean ± SEM; ***$P < 0.001$ *vs*. control. (C) Representative BLI images of the major internal organs photographed by using the IVIS system on Day 28. (D) The relative mouse body weight curves of the HYD-PEP06 groups and the control group. Data are presented as mean ± SEM; ***$P < 0.001$ by two-way ANOVA. (E) Animal survival curve and the survival duration of mice.

0.24-, and 0.17-fold, respectively; Table 2). The *ex vivo* organ images also supported that HYD-PEP06 inhibited the formation of lung metastasis with an inhibition rate of 87.8%, 92.7% and 95.3% at the dosage of 5, 10 and 20 mg/kg, respectively (Fig. 9C). In addition, HYD-PEP06 did not show any appreciable adverse effects with a stable increase in body weight of mice during the whole course of experiment (Fig. 9D). Of note, two mice of the control group died on Day 22 and three died on Day 26, while the HYD-PEP06 groups all survived to the end. That is, HYD-PEP06 prolonged the survival time of mice bearing tumors (Fig. 9E).

4. Discussion

In the present study, we provided strong evidence for the anti-HCC and lung metastasis-suppressing effects of HYD-PEP06 both *in vivo* with mouse models of tumor metastasis and postsurgical residual tumor xenograft and *in vitro* cellular models. Mechanically, HYD-PEP06 inhibited HCCLM3 cell metastasis and EMT likely by attenuating the PI3K/AKT pathway and hepatocellular CSC-like cells metastasis *via* suppressing the WNT/β-catenin signaling pathway. These findings suggest the potential of HYD-PEP06 as a novel therapeutic agent for HCC (Fig. 10).

HYD-PEP06 is an endostatin-derived synthetic polypeptide consisting of 30 amino acids engineered to attach RGD sequences to the N-terminus. Previous studies have demonstrated that HYD-PEP06 exhibits potent anti-tumor activity in diverse malignancies and is currently undergoing phase I clinical trial for evaluation of its safety and efficacy. Tuguzbaeva et al.[7] reported that HYD-PEP06 could inhibit the αv integrin/FAK/SRC signaling pathway and eliminate the cluster-driven metastasis of oral squamous cell carcinoma. Our previous study revealed that HYD-PEP06 significantly decreases the expression of miR-146b-5p through binding to integrin $\alpha v\beta 3$ with its RGD domain and inactivates the miR-146b-5p-Smad4 cascade to suppress colorectal carcinoma (CRC) pulmonary metastasis and residual tumor growth and increases the survival rate of tumor-bearing mice[6,40].

Table 2 Antitumor activity of HYD-PEP06 on mouse model of hepatocellular cancer pulmonary metastasis in nude mice.

Group	BLI flux (× 10^6 p/s)				IR (%)		
	Day 1	Day 14	Day 21	Day 28	Day 14	Day 21	Day 28
Control	28.12 ± 2.35	8.46 ± 2.57	81.01 ± 30.79	236.88 ± 88.10			
HYD-PEP06 5 mg/kg	28.67 ± 1.97	0.68 ± 0.12	1.25 ± 0.40*	9.83 ± 5.58***	91.9	98.5	95.8
HYD-PEP06 10 mg/kg	28.69 ± 2.31	0.69 ± 0.23	0.87 ± 0.26*	6.67 ± 2.78***	91.9	98.9	97.2
HYD-PEP06 20 mg/kg	28.32 ± 2.25	0.61 ± 0.11	0.51 ± 0.10*	4.77 ± 2.07***	92.7	99.4	98.0

The significance of differences (*vs*. control) was determined by two-way ANOVA followed by the Bonferroni procedure. Data are presented as mean ± SEM, $n = 10$; *$P < 0.05$, ***$P < 0.001$.
IR, inhibitory rate.

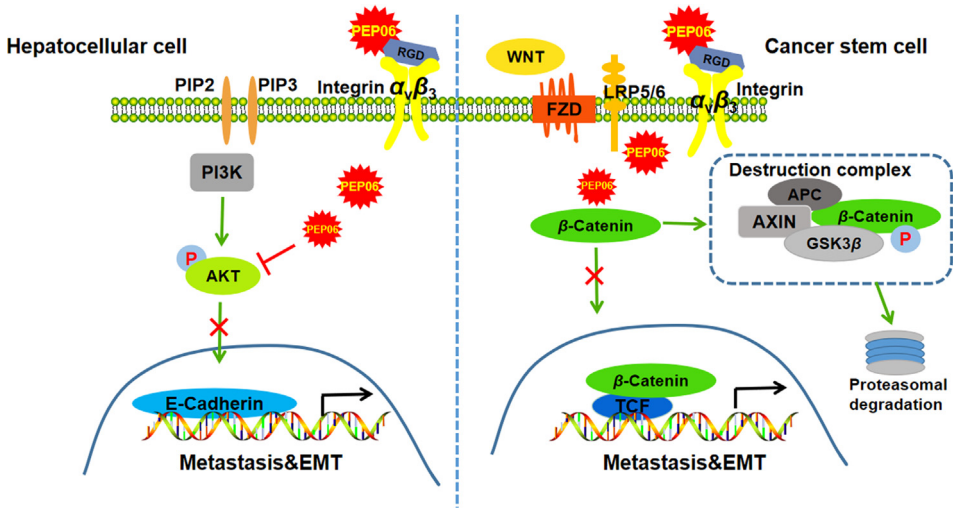

Figure 10 Mechanism diagram elaborating the underlying mechanism for the antitumor efficacy of HYD-PEP06 on HCC. HYD-PEP06 suppresses HCCLM3 metastasis *via* inhibiting EMT through suppressing the PI3K/AKT signaling pathway and increases survival time of lung metastasis. HYD-PEP06 attenuated metastasis capability and EMT of hepatocellular CSC-like cells *via* suppressing the WNT/β-catenin signaling pathway.

Endostatin, the prototype of HYD-PEP06, has been demonstrated to decrease the phosphorylation of AKT and inhibit growth and cell invasion in non-small cell lung cancer cells, breast cancer cells and esophagus cancer cells[41–43]. It is known that integrins can recognize RGD motif to affect cell adhesion through regulating the connection between cells and their microenvironment, which is one of the mechanisms by which HYD-PEP06 suppresses tumor metastasis[44]. Mounting evidence supports that HCC invasion and metastasis are positively regulated by multiple subtypes of integrins (αvβ3, α3β1, and α6β1) through multiple mechanisms, including cell adhesion, cell migration and cell invasion[45,46]. Moreover, the β subunit of integrin regulates the activity of AKT. For instance, inhibition of integrin αvβ3 significantly prevents the cathepsin B-induced activation of PI3K/AKT thereby the progression of HCC[47]. Ma et al.[48] reported that integrin αvβ3 suppresses HCC progression *via* targeting PI3K/AKT signaling. It is therefore possible that integrins underlies the inhibitory effects of HYD-PEP06 on HCC metastasis and EMT *via* inhibiting the PI3K/AKT pathway.

Epithelial to mesenchymal transition is a process tightly linked to CSC biology, including stemness, immune escape and resistance to radio- and chemotherapy[49]. When EMT is aberrantly activated, cancer cells can gain the stem cell-like characteristics attaining self-renewal capabilities and the potential to differentiate into literally all different cell types. The resulting cancer stem cells attain phenotypes of cancer including replicative immortality, resistance to cell death, and invasiveness. Tumor cells in the non-CSC subpopulation can spontaneously undergo EMT-like changes expressing CSC-like cell-surface marker genes and promoting tumor spread. EMT and mesenchymal to epithelial transition (MET) are mutually reversible in cancer cells, enabling the conversions between the CSCs and non-CSCs[50]. In our present study, we suggest that a subset of HepG2 cells displayed CSC-like biochemical and functional characteristics, leading to recurrence, metastasis and chemo-resistance of HCC. Besides, hyperactivity of the WNT/β-catenin signaling pathway is established as a cause of tumor development in some human malignancies. WNT/β-catenin also regulates the self-renewal of cancer stem-like cells and is involved in tumor progression and chemotherapy resistance[51]. This study also revealed that HYD-PEP06 inhibited liver CSCs by suppressing WNT/β-catenin signaling pathway.

CSCs, constituting <1% of the cellular population in the most solid tumors, are a rare subpopulation of highly self-renewal cells with intense tumorigenic potency and resistance to radio- and chemotherapy. Various oncogenic signaling pathways have been implicated in maintaining and regulating the function of CSCs in malignancies. Particularly, the dysregulated signaling pathways such as WNT/β-catenin, Notch, transformation growth factor β (TGF-β), hedgehog, Janus kinase/signal transducers and activators of transcription (JAK/STAT), PI3K/AKT, and NF-κB, have been well elucidated. Interestingly, miRNAs can modulate the expression and functioning of genes and their products associated with the abovementioned signaling pathways for the maintenance, growth, and function of CSCs. Upregulation of miR-19, miR-501-5p, and miR-744 stimulates the activation of β-catenin[52–54]. Conversely, upregulation of miR-708-5p and miR-142-3p inhibits β-catenin activation and prevents its accumulation in the cytoplasm[55,56]. Furthermore, upregulation of miR-21 and miR-23a stimulates the activation of the AKT/PI3K pathway, whereas upregulation of miR-128 inhibits its activation[57–59]. In addition, upregulation of miR-106b is found to act on TGF-β through targeting SMAD[60]. Downregulation of miR-200c stimulates the activation of Notch pathways and, hence, enhances CSC features[61]. Further, downregulation of miR-136 stimulates CSCs as a result of activating various signals including NF-κB, survivin, cyclin D1, and BCL2[62]. Taken together, stem cell features can be stimulated or suppressed by miRNA-regulated expression of signaling proteins. Our previous study has demonstrated that HYD-PEP06 significantly inhibited miR-146b-5p-SMAD4 cascade to suppressed CRC pulmonary metastasis. And this study showed that HYD-PEP06 suppressed HCC by inhibiting the PI3K/AKT pathway. Moreover, HYD-PEP06 exerted anti-metastasis effects in hepatocellular CSCs *via* suppressing WNT/β-catenin signaling pathway. However, whether miR-146b-5p also exerted therapeutic effect on HCC cells or regulate the stem cell features through these pathways needs further investigation.

5. Conclusions

This study uncovered that HYD-PEP06 possessed potent anti-HCC and anti-CSC metastasis effects by inhibiting EMT through downregulating the PI3K/AKT and WNT/β-catenin signal pathways. Our findings indicate that HYD-PEP06 might be considered as a potential drug for HCC treatment.

Acknowledgments

The authors gratefully acknowledge the financial support by the National Natural Science Foundation of China (Nos. 81770281, 81730012, and 81861128022).

Author contributions

Baofeng Yang, Yu Liu and Wenfeng Chu designed the experiments and supervised the project. Wei Tian was responsible for the manuscript writing and data analysis. Jiatong Li revised the manuscript. Zhuo Wang and Tong Zhang performed most *in vitro* experiments. Ying Han and Yanyan Liu conducted most *in vivo* experiments.

Conflicts of interest

The authors declare no conflicts of interest.

Appendix A. Supporting information

Supporting data to this article can be found online at https://doi.org/10.1016/j.apsb.2021.03.040.

References

1. Smith RA, Manassaram-Baptiste D, Brooks D, Doroshenk M, Fedewa S, Saslow D, et al. Cancer screening in the United States, 2015: a review of current American cancer society guidelines and current issues in cancer screening. *CA Cancer J Clin* 2015;**65**:30–54.
2. Keating GM. Sorafenib: a review in hepatocellular carcinoma. *Targeted Oncol* 2017;**12**:243–53.
3. Raoul JL, Kudo M, Finn RS, Edeline J, Reig M, Galle PR. Systemic therapy for intermediate and advanced hepatocellular carcinoma: sorafenib and beyond. *Cancer Treat Rev* 2018;**68**:16–24.
4. Mendez-Blanco C, Fondevila F, Garcia-Palomo A, Gonzalez-Gallego J, Mauriz JL. Sorafenib resistance in hepatocarcinoma: role of hypoxia-inducible factors. *Exp Mol Med* 2018;**50**:1–9.
5. Mozzanica N, Frigerio U, Negri M, Tadini G, Villa ML, Mantovani M, et al. Circadian rhythm of natural killer cell activity in vitiligo. *J Am Acad Dermatol* 1989;**20**:591–6.
6. Yu S, Li L, Tian W, Nie D, Mu W, Qiu F, et al. PEP06 polypeptide 30 exerts antitumour effect in colorectal carcinoma *via* inhibiting epithelial–mesenchymal transition. *Br J Pharmacol* 2018;**175**:3111–30.
7. Tuguzbaeva G, Yue E, Chen X, He L, Li X, Ju J, et al. PEP06 polypeptide 30 is a novel cluster-dissociating agent inhibiting alpha v integrin/FAK/Src signaling in oral squamous cell carcinoma cells. *Acta Pharm Sin B* 2019;**9**:1163–73.
8. Kalluri R, Weinberg RA. The basics of epithelial–mesenchymal transition. *J Clin Invest* 2009;**119**:1420–8.
9. Lee JM, Dedhar S, Kalluri R, Thompson EW. The epithelial–mesenchymal transition: new insights in signaling, development, and disease. *J Cell Biol* 2006;**172**:973–81.
10. Hanahan D, Weinberg RA. Hallmarks of cancer: the next generation. *Cell* 2011;**144**:646–74.
11. Nieto MA, Huang RY, Jackson RA, Thiery JP. Emt: 2016. *Cell* 2016;**166**:21–45.
12. Jou J, Diehl AM. Epithelial–mesenchymal transitions and hepatocarcinogenesis. *J Clin Invest* 2010;**120**:1031–4.
13. Xu Q, Liu X, Liu Z, Zhou Z, Wang Y, Tu J, et al. MicroRNA-1296 inhibits metastasis and epithelial–mesenchymal transition of hepatocellular carcinoma by targeting SRPK1-mediated PI3K/AKT pathway. *Mol Cancer* 2017;**16**:103.
14. Ren D, Yang Q, Dai Y, Guo W, Du H, Song L, et al. Oncogenic miR-210-3p promotes prostate cancer cell EMT and bone metastasis *via* NF-kappaB signaling pathway. *Mol Cancer* 2017;**16**:117.
15. Tang FY, Pai MH, Chiang EP. Consumption of high-fat diet induces tumor progression and epithelial–mesenchymal transition of colorectal cancer in a mouse xenograft model. *J Nutr Biochem* 2012;**23**:1302–13.
16. Zhang PF, Li KS, Shen YH, Gao PT, Dong ZR, Cai JB, et al. Galectin-1 induces hepatocellular carcinoma EMT and sorafenib resistance by activating FAK/PI3K/AKT signaling. *Cell Death Dis* 2016;**7**:e2201.
17. Bolos V, Peinado H, Perez-Moreno MA, Fraga MF, Esteller M, Cano A. The transcription factor Slug represses E-cadherin expression and induces epithelial to mesenchymal transitions: a comparison with Snail and E47 repressors. *J Cell Sci* 2003;**116**:499–511.
18. Qiao M, Sheng S, Pardee AB. Metastasis and AKT activation. *Cell Cycle* 2008;**7**:2991–6.
19. Wang Y, Shi J, Chai K, Ying X, Zhou BP. The role of snail in emt and tumorigenesis. *Curr Cancer Drug Targets* 2013;**13**:963–72.
20. Yoo YA, Kang MH, Lee HJ, Kim BH, Park JK, Kim HK, et al. Sonic hedgehog pathway promotes metastasis and lymphangiogenesis *via* activation of Akt, EMT, and MMP-9 pathway in gastric cancer. *Cancer Res* 2011;**71**:7061–70.
21. Zuo JH, Zhu W, Li MY, Li XH, Yi H, Zeng GQ, et al. Activation of EGFR promotes squamous carcinoma SCC10A cell migration and invasion *via* inducing EMT-like phenotype change and MMP-9-mediated degradation of E-cadherin. *J Cell Biochem* 2011;**112**:2508–17.
22. Clevers H. The cancer stem cell: premises, promises and challenges. *Nat Med* 2011;**17**:313–9.
23. Oikawa T. Cancer stem cells and their cellular origins in primary liver and biliary tract cancers. *Hepatology* 2016;**64**:645–51.
24. Mani SA, Guo W, Liao MJ, Eaton EN, Ayyanan A, Zhou AY, et al. The epithelial–mesenchymal transition generates cells with properties of stem cells. *Cell* 2008;**133**:704–15.
25. Wellner U, Schubert J, Burk UC, Schmalhofer O, Zhu F, Sonntag A, et al. The EMT-activator ZEB1 promotes tumorigenicity by repressing stemness-inhibiting microRNAs. *Nat Cell Biol* 2009;**11**:1487–95.
26. Pez F, Lopez A, Kim M, Wands JR, Caron de Fromentel C, Merle P. Wnt signaling and hepatocarcinogenesis: molecular targets for the development of innovative anticancer drugs. *J Hepatol* 2013;**59**:1107–17.
27. Yamashita T, Wang XW. Cancer stem cells in the development of liver cancer. *J Clin Invest* 2013;**123**:1911–8.
28. Liu ZH, Wang N, Wang FQ, Dong Q, Ding J. High expression of XRCC5 is associated with metastasis through Wnt signaling pathway and predicts poor prognosis in patients with hepatocellular carcinoma. *Eur Rev Med Pharmacol Sci* 2019;**23**:7835–47.
29. Zhang Q, Bai X, Chen W, Ma T, Hu Q, Liang C, et al. Wnt/beta-catenin signaling enhances hypoxia-induced epithelial–mesenchymal transition in hepatocellular carcinoma *via* crosstalk with HIF-1alpha signaling. *Carcinogenesis* 2013;**34**:962–73.
30. Rebouissou S, La Bella T, Rekik S, Imbeaud S, Calatayud AL, Rohr-Udilova N, et al. Proliferation markers are associated with MET expression in hepatocellular carcinoma and predict tivantinib sensitivity *in vitro*. *Clin Cancer Res* 2017;**23**:4364–75.
31. Zhang Y, Li D, Jiang Q, Cao S, Sun H, Chai Y, et al. Novel ADAM-17 inhibitor ZLDI-8 enhances the *in vitro* and *in vivo* chemotherapeutic effects of sorafenib on hepatocellular carcinoma cells. *Cell Death Dis* 2018;**9**:743.

32. Zhao H, Duan Q, Zhang Z, Li H, Wu H, Shen Q, et al. Up-regulation of glycolysis promotes the stemness and EMT phenotypes in gemcitabine-resistant pancreatic cancer cells. *J Cell Mol Med* 2017;**21**:2055−67.
33. Du B, Shim JS. Targeting epithelial−mesenchymal transition (EMT) to overcome drug resistance in cancer. *Molecules* 2016;**21**:965.
34. Lee SY, Jeong EK, Ju MK, Jeon HM, Kim MY, Kim CH, et al. Induction of metastasis, cancer stem cell phenotype, and oncogenic metabolism in cancer cells by ionizing radiation. *Mol Cancer* 2017;**16**:10.
35. Ye X, Weinberg RA. Epithelial−mesenchymal plasticity: a central regulator of cancer progression. *Trends Cell Biol* 2015;**25**:675−86.
36. Chen C, Song G, Xiang J, Zhang H, Zhao S, Zhan Y. AURKA promotes cancer metastasis by regulating epithelial−mesenchymal transition and cancer stem cell properties in hepatocellular carcinoma. *Biochem Biophys Res Commun* 2017;**486**:514−20.
37. Fan QM, Jing YY, Yu GF, Kou XR, Ye F, Gao L, et al. Tumor-associated macrophages promote cancer stem cell-like properties *via* transforming growth factor-beta1-induced epithelial−mesenchymal transition in hepatocellular carcinoma. *Cancer Lett* 2014;**352**:160−8.
38. Ma XL, Sun YF, Wang BL, Shen MN, Zhou Y, Chen JW, et al. Sphere-forming culture enriches liver cancer stem cells and reveals stearoyl-CoA desaturase 1 as a potential therapeutic target. *BMC Cancer* 2019;**19**:760.
39. Tabrizian P, Jibara G, Hechtman JF, Franssen B, Labow DM, Schwartz ME, et al. Outcomes following resection of intrahepatic cholangiocarcinoma. *HPB (Oxford)* 2015;**17**:344−51.
40. Dong X, Zhang Y, Meng Z, Zhu X, Gan H, Gu R, et al. A LC−MS/MS method to monitor the concentration of HYD-PEP06, a RGD-modified endostar mimetic peptide in rat blood. *J Chromatogr B Analyt Technol Biomed Life Sci* 2018;**1092**:296−305.
41. Liu L, Qiao Y, Hu C, Liu Y, Xia Y, Wang L, et al. Endostatin exerts radiosensitizing effect in non-small cell lung cancer cells by inhibiting VEGFR2 expression. *Clin Transl Oncol* 2016;**18**:18−26.
42. Zhang Y, Liu QZ, Xing SP, Zhang JL. Inhibiting effect of endostar combined with ginsenoside Rg3 on breast cancer tumor growth in tumor-bearing mice. *Asian Pac J Trop Med* 2016;**9**:180−3.
43. Liu GF, Chang H, Li BT, Zhang Y, Li DD, Liu Y, et al. Effect of recombinant human endostatin onradiotherapy for esophagus cancer. *Asian Pac J Trop Med* 2016;**9**:86−90.
44. Ruoslahti E. RGD and other recognition sequences for integrins. *Annu Rev Cell Dev Biol* 1996;**12**:697−715.
45. Torimura T, Ueno T, Kin M, Harada R, Nakamura T, Kawaguchi T, et al. Autocrine motility factor enhances hepatoma cell invasion across the basement membrane through activation of beta1 integrins. *Hepatology* 2001;**34**:62−71.
46. Yang C, Zeisberg M, Lively JC, Nyberg P, Afdhal N, Kalluri R. Integrin alpha1beta1 and alpha2beta1 are the key regulators of hepatocarcinoma cell invasion across the fibrotic matrix microenvironment. *Cancer Res* 2003;**63**:8312−7.
47. Xu ZZ, Xiu P, Lv JW, Wang FH, Dong XF, Liu F, et al. Integrin alphavbeta3 is required for cathepsin B-induced hepatocellular carcinoma progression. *Mol Med Rep* 2015;**11**:3499−504.
48. Ma WL, Jeng LB, Lai HC, Liao PY, Chang C. Androgen receptor enhances cell adhesion and decreases cell migration *via* modulating beta1-integrin-AKT signaling in hepatocellular carcinoma cells. *Cancer Lett* 2014;**351**:64−71.
49. Najafi M, Mortezaee K, Majidpoor J. Cancer stem cell (CSC) resistance drivers. *Life Sci* 2019;**234**:116781.
50. Wang H, Unternaehrer JJ. Epithelial−mesenchymal transition and cancer stem cells: at the crossroads of differentiation and dedifferentiation. *Dev Dynam* 2019;**248**:10−20.
51. Martins-Neves SR, Paiva-Oliveira DI, Fontes-Ribeiro C, Bovee J, Cleton-Jansen AM, Gomes CMF. IWR-1, a tankyrase inhibitor, attenuates Wnt/beta-catenin signaling in cancer stem-like cells and inhibits *in vivo* the growth of a subcutaneous human osteosarcoma xenograft. *Cancer Lett* 2018;**414**:1−15.
52. Zhu J, Wang S, Chen Y, Li X, Jiang Y, Yang X, et al. miR-19 targeting of GSK3beta mediates sulforaphane suppression of lung cancer stem cells. *J Nutr Biochem* 2017;**44**:80−91.
53. Fan D, Ren B, Yang X, Liu J, Zhang Z. Upregulation of miR-501-5p activates the Wnt/beta-catenin signaling pathway and enhances stem cell-like phenotype in gastric cancer. *J Exp Clin Cancer Res* 2016;**35**:177.
54. Khan AQ, Ahmed EI, Elareer NR, Junejo K, Steinhoff M, Uddin S. Role of miRNA-regulated cancer stem cells in the pathogenesis of human malignancies. *Cells* 2019;**8**:840.
55. Liu T, Wu X, Chen T, Luo Z, Hu X. Downregulation of DNMT3A by miR-708-5p inhibits lung cancer stem cell-like phenotypes through repressing Wnt/beta-catenin signaling. *Clin Cancer Res* 2018;**24**:1748−60.
56. Troschel FM, Bohly N, Borrmann K, Braun T, Schwickert A, Kiesel L, et al. miR-142-3p attenuates breast cancer stem cell characteristics and decreases radioresistance *in vitro*. *Tumour Biol* 2018;**40**. 1010428318791887.
57. Mamoori A, Gopalan V, Smith RA, Lam AK. Modulatory roles of microRNAs in the regulation of different signalling pathways in large bowel cancer stem cells. *Biol Cell* 2016;**108**:51−64.
58. Han Z, Zhou X, Li S, Qin Y, Chen Y, Liu H. Inhibition of miR-23a increases the sensitivity of lung cancer stem cells to erlotinib through PTEN/PI3K/Akt pathway. *Oncol Rep* 2017;**38**:3064−70.
59. Kwon T, Chandimali N, Huynh DL, Zhang JJ, Kim N, Bak Y, et al. BRM270 inhibits cancer stem cell maintenance *via* microRNA regulation in chemoresistant A549 lung adenocarcinoma cells. *Cell Death Dis* 2018;**9**:244.
60. Yu D, Shin HS, Lee YS, Lee YC. miR-106b modulates cancer stem cell characteristics through TGF-beta/Smad signaling in CD44-positive gastric cancer cells. *Lab Invest* 2014;**94**:1370−81.
61. Huang CC, Lin CM, Huang YJ, Wei L, Ting LL, Kuo CC, et al. Garcinol downregulates Notch1 signaling *via* modulating miR-200c and suppresses oncogenic properties of PANC-1 cancer stem-like cells. *Biotechnol Appl Biochem* 2017;**64**:165−73.
62. Jeong JY, Kang H, Kim TH, Kim G, Heo JH, Kwon AY, et al. MicroRNA-136 inhibits cancer stem cell activity and enhances the anti-tumor effect of paclitaxel against chemoresistant ovarian cancer cells by targeting Notch3. *Cancer Lett* 2017;**386**:168−78.